International Journal of Concrete Structures and Materials

RESEARCH Open Access

Flexural Behavior of Reactive Powder Concrete Ferrocement Hollow Beams Reinforced by Different Mesh Type

M. Alaa[1], Mohamed H. Makhlouf[1*], M. H. Mansour[1] and K. M. Elsayed[1]

Abstract

In fact, the non-economic design of concrete structures is becoming a big challenge. Therefore, the objective of this research is to investigate the flexural behavior of ferrocement hollow beams experimentally and analytically. To achieve this objective, five specimens of reinforced concrete beams were prepared and tested under a single-point-loading system until failed. The beams have clear spans of 1500 mm and cross-section dimensions of 100 * 200 * 1600 mm. The ferrocement beams were strengthened with either welded wire mesh (WWM) or expanded metal mesh (EMM) and have an extruded foam core (EFC). The structural behaviors of the studied beams, including the measurements of first crack, deflection, ultimate load, failure mode, crack pattern, and ductility index, were investigated. In addition, finite-element model (ABAQUS) was validated using the experimental data. The results indicated that the use of a second layer of expanded steel mesh reinforcement in ferrocement beams was found to significantly enhance their performance. The addition of this reinforcement resulted in an increase in the ultimate load capacity and maximum deflection by 11.38% and 2.92%, respectively. Moreover, the finite-element models created using the ABAQUS finite-element program were validated against the experimental data. The comparison between the nonlinear finite-element (NLFE) ultimate loads and the experimental ultimate loads, with an average ratio of 0.96, varies between 0.94 and 0.98 in the numerical results. This indicates that the numerical models accurately predicted the beams' behavior.

Keywords Ferrocement, Flexural strength, Expanded wire mesh, Welded wire mesh, Nonlinear finite-element analysis

1 Introduction

Ferrocement, a thin-walled reinforced concrete, is composed of hydraulic cement mortar and continuous, relatively small-scale wire mesh layers for reinforcement. The wire mesh layers can be constructed from metallic or other appropriate materials (ACI 549-1R-88, 2006). Cost-effective housing can be built with relatively light prefabricated structural elements that can be sculpted into interesting architectural shapes thanks to the application of ferrocement. Ferrocement has been used in the construction and repair of buildings, tanks, roofs, silos, and other structures for concrete reinforcement (Gaidhankar et al., 2017a; Shaheen, 2022; Usman & Shaharudin, 2018). Ferrocement is mostly used for strengthening reinforced concrete beams, columns, and slabs (Kaish et al., 2018; Shaaban et al., 2018a; Yardim, 2019).

The flexural behavior of hollow core ferrocement elements was studied by a number of researchers. For instance, Chandra Sekhar Rao et al. (2012) published the results of an experimental program made to study how ferrocement box beams behaved when subjected to flexural loading. The project involved casting and bending tests on eight ferrocement box beams. Cored

Journal information: ISSN 1976-0485 / eISSN 2234-1315.

*Correspondence:
Mohamed H. Makhlouf
mohamed.makhlouf@bhit.bu.edu.eg
[1] Civil Department, Benha Faculty of Engineering, Benha University, Benha, Egypt

beams' flexural strength was contrasted with that of solid box beams. According to the test results, the member's weight loss was greater than the reduction in flexural strength caused by the vacancies. The post-ductility of the member improved with a rise in the number of layers, which in turn improved the moment curvature response of the cored specimens under flexural loading.

The flexural strength of reinforced concrete beams with steel slag and laminates made of ferrocement used as a partial substitute for fine aggregates was examined by Basil S. Al-Shathr et al. (2022). Two samples of two-volume mesh fractions (18.8% and 2.36%) and two quantities of steel slag reinforcement (0% and 32%) were put to the test. These samples included four ferrocement laminate beams and five RC beams with dimensions of 1220 × 100 × 150 mm (galvanized square welded wire mesh with a 3 mm wire diameter was employed and strengthened with epoxy resin). Two-point loading was used to test each sample. When subjected to flexural load, the load-carrying capacity of ferrocement beams with a volume fraction proportion of 2.36% and 32% steel slag rose dramatically, reaching 83%, according to the authors, in addition to increasing other properties like ductility and energy absorption capacity.

Research on the flexural characteristics of a ferrocement U-shaped channel section reinforced with wire mesh with variable numbers of wire mesh layers was carried out by Gaidhankar et al. (2017b) using experimental and finite-element methods. Ansys was used to analyze a ferrocement U-shaped channel with varying mesh thicknesses and layers. They discovered that when the number of mesh layers grows from 2 to 4, flexural strength and load-carrying capacity do as well.

E.H. Fahmy examined the effects of steel mesh type and quantity on beam performance in U-formed ferrocement forms (Fahmy et al., 2014a). The properties of thin composite elements constructed of ferrocement with stainless steel and E-fiber glass meshes under flexural were investigated by El-Wafa and Fukuzawa (2010). Their factors included the impact of mesh type, mesh layer count, mesh wire sizes in relation to opening size, and mortar type. They claimed that because stainless steel meshes had crack patterns that consisted of several small, evenly spaced fissures, they displayed better bending behavior. To improve the structural behavior of flexural reinforced concrete beams, Shaaban (2002) looked into the viability of using ferrocement as a permanent formwork. Using expanded wire fabrics as a continuous formwork and adding wings made of the same material, he found that the beams' load capacity increased by 22% and their crack widths fell by 36%. Fahmy et al. (2014b) looked at the U-shaped ferrocement formwork's beam performance, concerning the type and quantity of steel mesh layers. The findings showed that these beams had superior fracture control, high ductility, and enhanced energy absorption under high ultimate and serviceability loads. Shaheen et al. looked at how apertures affected the structural behavior of ferrocement I-beams reinforced with metal and non-metal meshes, two distinct types of reinforcing mesh. The findings indicated that in terms of ultimate loads, deflections, ductility ratios, and energy absorption, welded steel mesh reinforced beams performed better than geo-grid mesh reinforced beams (Shaheen et al., 2022). Elkassas et al. looked at the flexural behavior of empty steel beams reinforced with ferrocement layers in precast lightweight composite beams. In comparison to the control specimen, the test findings showed that a 30 mm layer of ferrocement increased the capacity by 18% (Elkassas et al., 2022). In their study, Taha et al. (2022) used locally made hybrid-GFRP (H-GFRP) bars and steel wires to test and analyze the flexural performance of HSC beams with a compressive strength of 60 MPa. According to the test results, H-GFRP bars display a ductile failure mode and the same mechanical failure mechanism as reinforcing steel bars when they reach their maximum capacity. Furthermore, the ultimate loads of beams reinforced with standard GFRP bars and steel are lower than those of beams reinforced with H-GFRP bars. A hollow ferrocement beam of self-compacting mortar reinforced with various forms of non-metallic (GFRP bars, fiber glass mesh) and metallic (steel bars) reinforcement was one type of ferrocement that Qutaiba Najm and Aziz (2022) studied. The results showed that the loads for hollow ferrocement beams reinforced with GFRP bars and several layers of fiber glass mesh (one, two, and three) were higher by 7.51%, 9.88%, and 5.15%, respectively. An experimental and mathematical study of the behavior of ferrocement composite tanks under static pressure loads was conducted by Taha et al. (2023a). According to the experimental data, the failure load of ferrocement composite tanks is higher than that of conventionally reinforced concrete tanks, especially those reinforced with fiberglass polymer mesh. Taha et al.'s (2023b) investigation of the flexure behavior of geopolymer ferrocement beams under axial flexural stress involves both experimental and computational methods. The test results showed that the specimens tested with ferrocement had ultimate loads that were about 15% less than those of the control group. Initial fractures, ultimate loads, energy absorption, and ductility index all improved as the volume percent of the wire mesh reinforcement increased. However, a great deal of research has been done on the structural behavior of RC elements that have been strengthened with ferrocement (Abdullah & Abdulla, 2023; El-Sayed & Algash, 2021; El-Sayed et al., 2023a, 2023c, 2023d; Makhlouf et al., 2024). It is

often observed that the primary reinforcement in slabs, beams, columns, and stirrups, as well as when appropriate cover is not maintained and reinforcement is exposed in the cover region, are the areas of RC structures most commonly affected by corrosion. To restore the original strength of the RC, patchwork repair can be performed on damaged concrete surfaces in slabs, beams, and columns using ferrocement. The method of cement patch repair can be applied to the roof of slabs, bottom and middle sections of beams, columns, etc.

2 Research Signification

The principal aim of this study is to examine the behavior of lightweight reinforced concrete beams reinforced with different metal mesh reinforcement materials as a potential substitute for ordinary reinforced concrete beams. Two types of steel mesh (expanded steel wire mesh and welded wire mesh) are used in different layers to reinforce such low-weight beams. The suggested beams have a lower weight than typical beams made of reinforced concrete. This study looked at the type of concrete utilized, the quantity of steel reinforcement used, and the kind of steel reinforcement. A theoretical study will be carried out using the finite-element program ABAQUS to validate the results of the experimental program.

3 Experimental Program

To determine whether creating structural ferrocement beam forms filled with core material is a feasible substitute for traditional reinforced concrete beams, this research's experimental program was created, and the experimental program was run in the laboratory of Benha University in Egypt's Faculty of Engineering. Examining the flexural behavior of reactive powder concrete ferrocement specimens reinforced with welded and expanded wire mesh, as well as with light-weight core material, in contrast to control specimens composed of both concrete and reactive powder concrete, was the main goal of the study. For every specimen, the ductility index, ultimate load, deflection, first crack, and crack pattern were recorded. The mode of failure at collapse was also noted.

3.1 Materials

Fine Aggregate: It was siliceous sand found naturally. Its features meet ASTM C/136-84a's requirements. It had a specific gravity of 2.65 and a coefficient of fineness of 2.55, and was practically impure-free (ASTM C778).

Coarse Aggregate: It was crushed dolomite with a specific gravity of 2.75, a crushing modulus of 18.5%, and a water absorption of 2.1% that complied with Egyptian Code 203/2007. These particles have a relatively low proportion of flat particles and an erratic, angular form (Egyptian standards specification, 2012).

Quartz Sand: Quartz sand with a specific gravity of 2.65 and particle sizes ranging from 1.18 to 2.36 mm was employed in this study.

Quartz Powder: Quartz sand with a mean particle size of 10–15 μm was utilized in this study and was supplied by a local Egyptian company.

Cement: According to ASTM C/150–07, it was normal Portland cement of grade 42.5N, compliant with Type I Portland cement (ASTM, 2007).

Silica Fume (S.F): It is used to make standard concrete and ferrocement mortar stronger. It was imported from the Sika firm in Egypt and used in mortar formulations as a partly weight-for-weight replacement for cement.

Extruded Foam Core (EFC): According to ASTM C578, foam sheets are thermal insulation boards made from premium extruded polystyrene foam and come in a variety of thicknesses and edge configurations. El-Hager Pack Company manufactures foam in Egypt.

It functioned as the main element of the specimens in Group E. This white board is 2×1 m and was created using continuous extrusion. It has special qualities like great water resistance, low heat conductivity, strong compressive strength, and a density of 38 kg/m^3.

Water: It was safe for drinking, devoid of contaminants that would compromise the strength and concrete's resilience, and perfect for mixing concrete.

Superplasticizer: It is ASTM C 494/C494M compliant (ASTM, 2005) and has a room-temperature density of 1.21 kg/liter. Two dosages of the superplasticizer were applied. Visco Crete-1000 RM from the Sika Company in Egypt has been used in the typical dose for greater feasibility without lowering the water content, which is 0.15–0.30% of the cement weight (or roughly 0.6 kg/m^3 of concrete).

Reinforcing Steel: The longitudinal steel reinforcement used in all specimens is 10 mm-diameter elevated tensile-distorted bars with a nominal yield strength of 360 N/mm2. For the control beams, shear reinforcement in the form of mild steel stirrups with a nominal yield strength of 240 N/mm2 and a diameter of 6 mm were utilized.

Mesh Reinforcement: The reinforcement for the ferrocement beams is made of expanded metal mesh (EMM) and square welded wire steel mesh (WWM), both of which are readily available in local markets. The meshes' characteristics are listed in Table 1. Fig. 1 displays the steel meshes as seen through a camera.

3.2 Concrete and Mortar Matrix

Table 2 displays the weight-per-cubic-meter mix proportions for the regular weight concrete used for specimen D1. The reactive powder concrete (ferrocement

Table 1 Steel mesh's geometric and physical characteristics

Mesh type	Mesh entrance (mm)		Dim. of strands (mm)		Diameter (mm)	Size of grid (mm)	Weight (gm/m^2)	Proof stress (MPa)
	Long way	Short way	Width	thickness				
WWM	–	–	–	–	0.8	12.5*12.5	320	400
EMM	35	18	2	1			630	199

(a) Expanded metal mesh (b) Welded wire mesh

Fig. 1 Various mesh types are used as reinforcement (Makhlouf et al., 2024)

Table 2 Proportions of a typical concrete mix by weight for D1 specimen

Material	Cement	Coarse aggregate	Fine aggregate	Water	Superplasticizer
Weight (Kg/m^3)	560	1090	586	168	6

mortar) used for specimen D2, and specimens of group E (ferrocement beams). Table 3 displays the mortar mix proportions that were utilized to generate the ferrocement for specimen D2, and specimens of group E, which were developed in compliance with ACI 549.1R-93 & ACI 549-1R-88 (549–1R-88, A. C. I.). Superplasticizer was added to mortar mixtures in the proper quantity to increase workability. Three cubes, each measuring 70*70*70 mm, were cast for the ferrocement mortar mix and the regular concrete mix to test the strength of the mixtures.

For normal concrete, the compressive strength is 54.73 MPa. The compressive strength of the mortar used to prepare the ferrocement beams is 64.4 MPa.

3.3 Samples Description

Five composite beams with simple supports and similar dimensions of 100 * 200 * 1600 mm make up the experimental program. The specimens were tested under a single-point-loading system. Two groups (D and E) were made out of the specimens. Group D (control beams) beams were cast with a conventional concrete beam for D1 and a reactive powder concrete beam for D2. Group E beams were constructed using EFC, a reinforced extruded foam core. The usual size and reinforcement of the examined materials are displayed in Fig. 2. Fig. 3 displays the cross-sectional characteristics of the beams. The details about the test specimens are collected in Table 4.

3.4 Preparation of Test Specimen

A wooden form intended to cast two elements at once was used to cast the specimens. The beam that was taken out of the form, the primary wire mesh cage, and the ferrocement cores coated by EMM and WWM, and the form are all shown in Fig. 4. After assembling the wooden form, adding strengthening caging to the form, and applying a thin layer of shuttering oil, the beams were cast. After the mortar was poured and vibrated in the form until it reached a thickness

Table 3 Proportions of the ferrocement mortar mix by weight for D2, E1, E2, and E3 specimens

Material	Cement	Silica fume	Quartz sand	Quartz powder	Water	Superplasticizer
Weight (Kg/m^3)	560	235	885	220	200	6

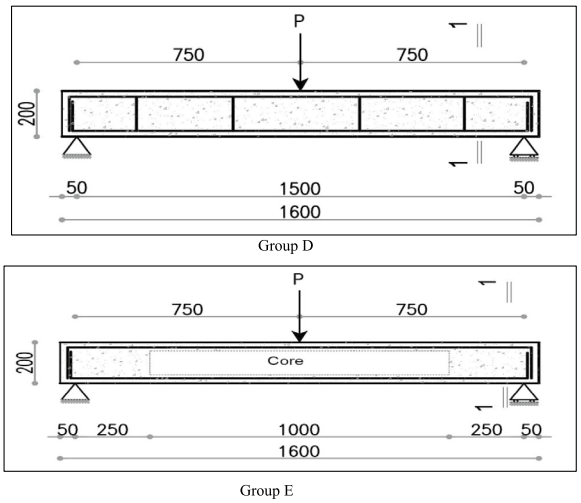

Fig. 2 Ideal dimensions and reinforcement of the tested specimens (all dimensions in millimeters)

of 50 mm, reinforcing caging was applied to adequately cover the steel wire mesh in the ferrocement beams. Cure spacers were then pressed into the mortar layer. After the caging was inserted into the form, the mortar matrix for ferrocement beams or concrete for control beams was added. An electrical vibrator was then used to make sure correct compaction and remove any air gaps. Before deconstructing the form, the ferrocement forms were kept inside for 24 h. All of the preceding stages are seen in Fig. 4.

3.5 Test Setup

A system of single-point loading was used to test every beam. At the test beam's mid-span, a linear variable displacement transducer (LVDT) was utilized to track deflection at the load application location, as shown in Fig. 5. White emulsion was used to paint the beams to make it easy to see the patterns of the cracks. The specimens were correctly positioned in the loading frame before the test began. To ensure that all of the equipment was functioning, a minor load was first applied. The load was then steadily raised until the specimen failed.

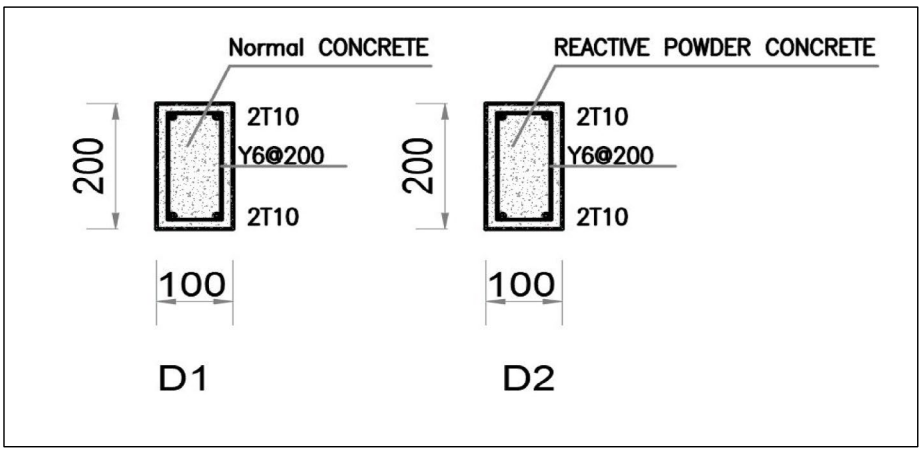

a) Group (D) control specimens

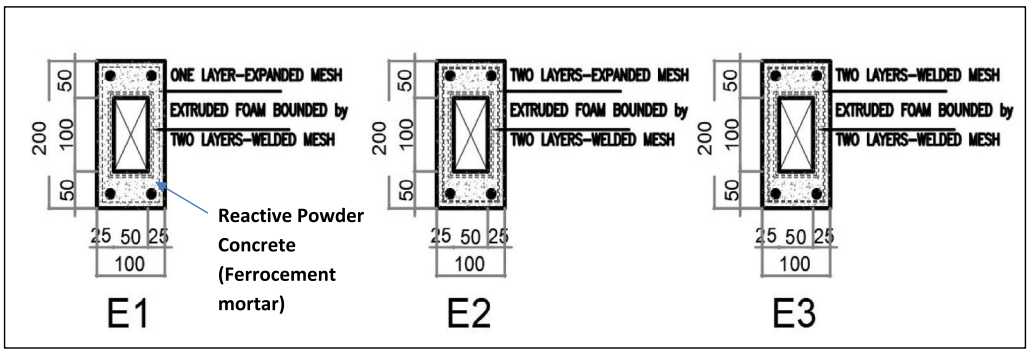

b) Group (E)

Fig. 3 Typical cross sections of tested specimens

Table 4 Specifications of the samples

Group	Specimen name	Specimen's core type	Links	No. of layers	Kind of mesh
D	D1		5 $^{\varphi}$6/m		
	D2		5 $^{\varphi}$6/m		
E	E1	EFC			EMM
	E2	EFC			EMM
	E3	EFC			WWM

Deflections were automatically recorded at each load increment using a computerized data acquisition (DAQ) system. Each load increment also included a comment about the crack pattern. Excessive cracking at the beam's shear span, where the applied load was lower and the deflection was higher, revealed the ultimate load.

4 Experimental Results and Discussion

Among the structural characteristics that were looked at were the failure mechanism, fracture pattern, ductility index, first crack load, ultimate load, deflection at the first crack load, and deflection at the ultimate load. The load–deflection curves for the items under examination were also sketched. The curve deviates from its initial linear connection at the point of deflection at the first crack load, also known as the first crack initiation. The deflection at ultimate loads divided by the deflection at the first crack is known as the ductility index. A beam has more warnings before it ultimately collapses, according to a beam with a higher ductility index value. The values listed above are listed in Table 5.

4.1 Load–Deflection Relationships

Generally, ferrocement specimens with light-weight core material had higher resistance than the control specimens D1 (normal concrete) and D2 (reactive powder concrete), according to the study conducted by Shaaban et al. (2018b).

The ultimate loads and maximum deflection of ferrocement specimens with light-weight core material are higher than the corresponding values of normal concrete specimens (D1) by a range of 8 to 11.5% for ultimate loads and by a range of 1.7% to 11.4% for maximum deflection.

The ultimate loads of ferrocement specimens with light-weight core material are higher than the corresponding values of reactive powder concrete specimens (D2), except for specimens (E1–1E and E3–2W).

The specimen (E2–2E) revealed the highest ultimate load and maximum deflection values by 14.8% and 18.6%, respectively, compared to specimen D2.

The next sections address how the tested specimens behaved in reference to the load–deflection relationship.

4.1.1 Control Specimens

The comparison between the load–deflection relationships of the two specimens (D1 and D2) did not show a significant difference. Fig. 6 shows the load–deflection curves of the control specimen for the normal concrete beam (D1) and the ferrocement beam (D2). Group D, from the figure, has an ultimate load for specimen (D1) that is less than that of specimen (D2). The percentage decrease in the ultimate load is 10.81%. Also, the deflection of specimen (D2) increases by 12.96% compared to specimen (D1). As Shaaban et al. (2018a) noted, this is because different types of concrete have varied properties.

4.1.2 The Effect of Steel Mesh Type

According to the laboratory results, the use of expanded metal mesh (EMM) is better than the use of welded wire mesh (WWM) and gives better results in ultimate loads and maximum deflection. The specimen (E2–2E) revealed the highest ultimate load and maximum deflection values compared to all tested specimens. To evaluate the reinforced steel mesh type at beams with the same core, specimens reinforced with welded wire mesh and expanded steel mesh were compared to the control specimen (D2). Fig. 7 displays the load–deflection curves of the control specimen (D2) compared to the specimens for group (E), which are reinforced with one layer of EMM (E1), two layers of EMM (E2), and two layers of WWM (E3). From the figure, the ultimate load for specimen E2 is greater than that of specimens D2, E1, and E3. This is due to the type of mesh. The percentage of increase in ultimate load is 1.80%, 11.22%, and 3.81%, respectively. Also, the deflection of specimen (D2) is greater than that of specimens (E1, E2, and E3); the percentage increase in deflection is 31.35%, 8.81, and 10.51%, respectively. The findings accord with the studies conducted by Shaaban et al. (2018a).

4.2 Crack Patterns

All of the specimens finally collapsed due to flexural stresses. All tested specimens' crack patterns are shown in Fig. 8. All examined beams first developed vertical cracks, also known as flexural cracks, in the mid-span region. The last flexural crack in the shear span region became inclined and crossed mid-depth, which was the abrupt beginning of the diagonal crack that caused failure. Due to dowel action, the cracks then spread concurrently throughout the tensile reinforcement in the direction of the load point and the support, resulting in a loss of bond and beam failure. For beams without wire mesh, the diagonal cracking load was nearly equal to the failure load. Depending on

a) Wooden form design

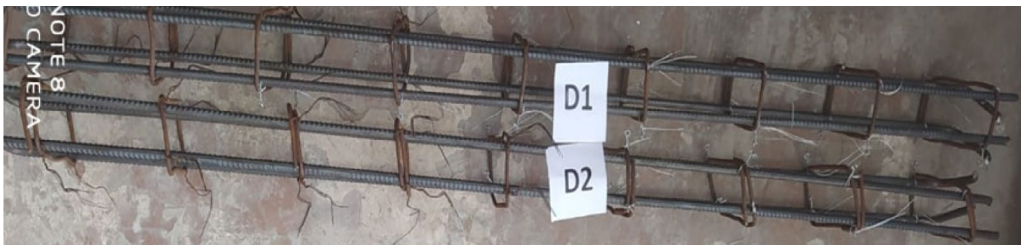

b) Reinforcement of group D

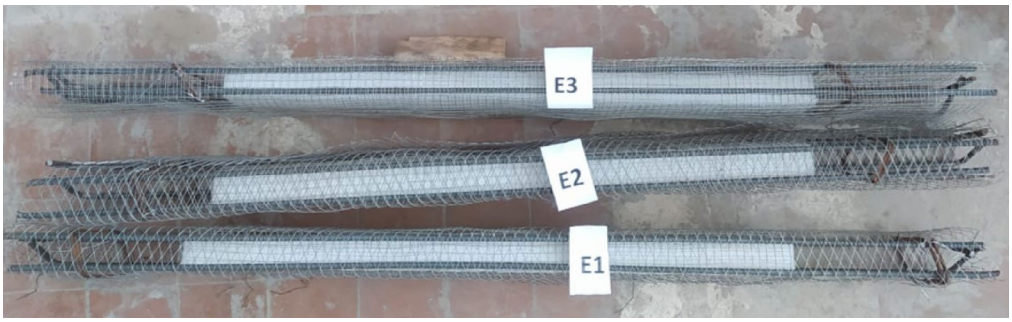

c) Reinforcement of group E

d) Molded beams.

Fig. 4 Steps of specimen's preparation

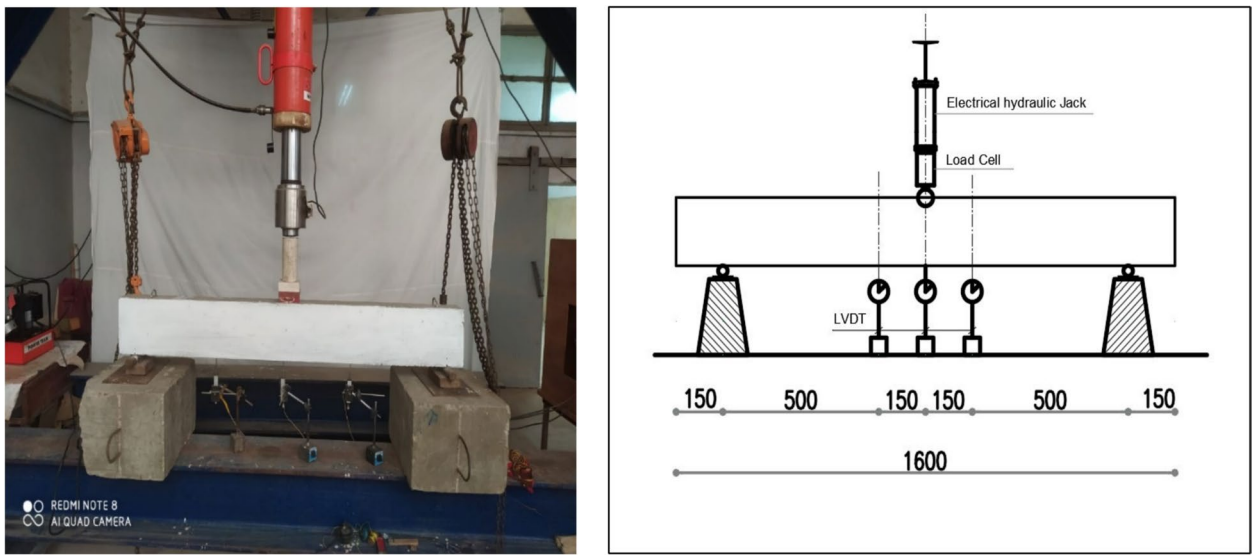

Fig. 5 Test specimen setup

Table 5 Experimental results

Group	Specimens designation	First crack load, KN	Ultimate load, KN	Def. at first crack load, mm	Def. at ultimate load, mm	Ductility index
D	D1	14.87	47.25	1.49	12.96	8.69
	D2	15.82	52.36	1.74	14.64	8.41
E	E1-1E	11.24	47.94	1.21	10.05	8.30
	E2-2E	13.3	53.32	1.55	13.35	8.61
	E3-2W	15.68	51.36	1.61	13.1	8.13

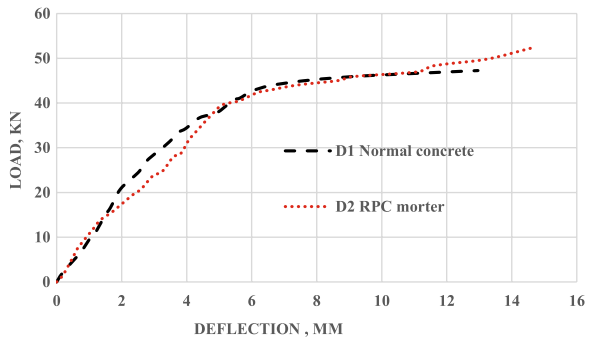

Fig. 6 Load–deflection curves for specimens of Group (D)

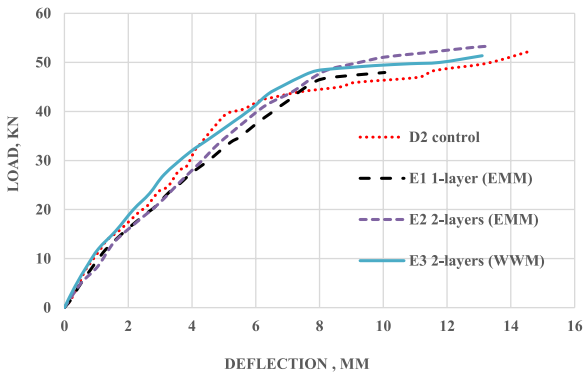

Fig. 7 The effect of steel mesh type on the load–deflection curves

the number of layers utilized, diagonal cracks may not emerge until a beam with wire mesh fails. Fig. 8 shows that as the number of web wire mesh layers increased, so did the number of small diagonal cracks in the shear span.

5 Theoretical Prediction of Test Beam Ultimate Loads

Using finite-element modeling, empirical solutions, and mathematical modeling, several studies have reported on the prediction of ultimate loads and ultimate moment capacity for ferrocement structural elements (Eskandari &

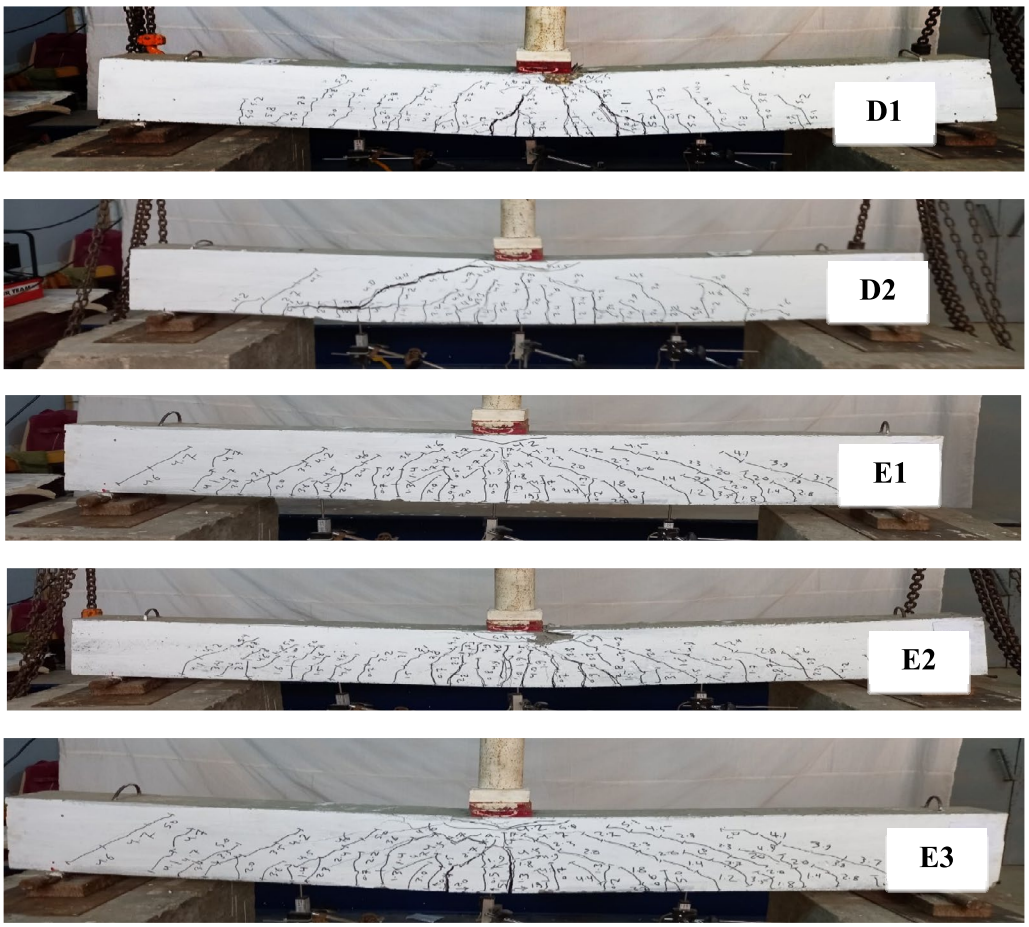

Fig. 8 Cracking patterns of tested beams

Madadi, 2015; Gandomi et al., 2013; Mhadeshwar & Naik, 2017). The method used by Fahmy et al. (2014a) was followed in this study to compute the theoretical ultimate moment of the ferrocement beams.

The following fundamental presumptions were made to calculate the ultimate moment:

a) Strains in the concrete core, mortar matrix, and reinforcement are directly proportional to the distances from the neutral axis, as shown in Fig. 9.
b) Failure occurs when the ferrocement mortar's maximum compressive strain reaches 0.003.
c) At the ultimate load, the compressive contribution is represented by a rectangular stress bock with a depth of (a) and a maximum stress of (0.67 fcu), and the tensile contribution is ignored.

Considering the strain and forces distribution diagram (Fig. 9) at equilibrium

$$\boldsymbol{Cc} = \boldsymbol{T} \tag{1}$$

$$\boldsymbol{Cc} = a \times b \times fcu, \tag{2}$$

where $a = 0.80 \times c$ according to Egyptian code of practice

$$\boldsymbol{T} = \Sigma \boldsymbol{Tri} = \boldsymbol{Tr1} + \boldsymbol{Tr2} + \boldsymbol{Tr3} + \boldsymbol{Tr4} + \boldsymbol{Tr5} + \boldsymbol{Tr6} + \boldsymbol{Tr7} \tag{3}$$

$$\boldsymbol{Tr7} = \boldsymbol{\sigma} m.bot. \times \boldsymbol{Am.bot.} \tag{4}$$

$$\boldsymbol{Tr6} = \boldsymbol{\sigma} st.bot. \times \boldsymbol{Ast.bot.} \tag{5}$$

$$\boldsymbol{Tr5} = \boldsymbol{\sigma} c.m..\boldsymbol{bot.} \times \boldsymbol{Ac.m.bot} \tag{6}$$

$$\boldsymbol{Tr4} = \boldsymbol{\sigma} m.web \times \boldsymbol{Ac.m.web} \times No.ofwebs \tag{7}$$

$$\boldsymbol{Tr3} = \boldsymbol{\sigma} c.m..top \times \boldsymbol{Ac.m.top} \tag{8}$$

$$\boldsymbol{Tr2} = \boldsymbol{\sigma} st.top \times \boldsymbol{Ast.top} \tag{9}$$

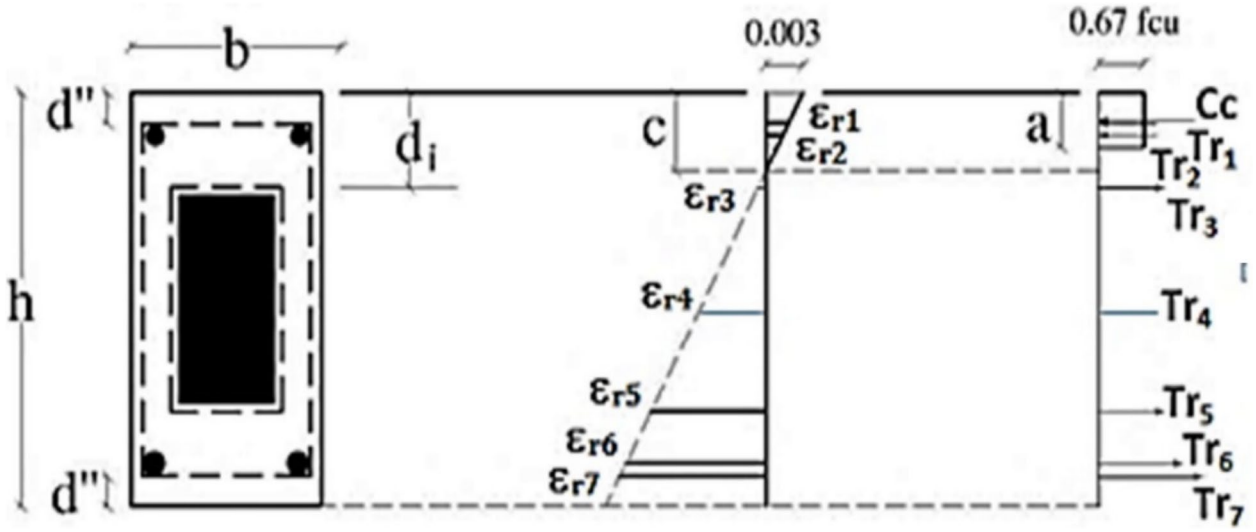

Fig. 9 Strain and forces' distribution of ferrocement beam section under bending (Fahmy et al., 2014a)

$$Tr1 = \sigma m.top \times Am.top \tag{10}$$

$$Ari = \eta \circ \times Vfi \times Ac \tag{11}$$

$$\sigma st.bot. = Es \times \varepsilon s.bot. \leq Fysif\,(\varepsilon s.bot. \leq \varepsilon y.s.) \tag{12}$$

$$\begin{aligned} \sigma st.bot. &= Fys + Esth \times (\varepsilon s.top.\varepsilon y.s.) \\ &\leq Fuif\,(\varepsilon s.bot. > \varepsilon y.s.) \end{aligned} \tag{13}$$

$$\sigma st.top = Es \times \varepsilon s.top \leq Fysif\left(\varepsilon s.top \leq \varepsilon y.s.\right) \tag{14}$$

$$\begin{aligned} \sigma st.top &= Fys + Esth \times (\varepsilon s.top.\varepsilon y.s.) \\ &\leq Fuif\,(\varepsilon s.top > \varepsilon y.s.) \end{aligned} \tag{15}$$

$$\sigma m.web = Es \times \varepsilon m.web \leq Fym \tag{16}$$

$$\sigma m.bot. = Es \times \varepsilon m.bot. \leq Fym \tag{17}$$

$$\sigma m.top = Es \times \varepsilon m.top \leq Fym. \tag{18}$$

The geometry of the strain distribution illustrated in Fig. 6 can be used to determine the strain at the top steel bars, bottom steel bars, web steel reinforcement mesh, and bottom steel reinforcement mesh (εs.top ,εs.bot ,ε m.web,εm.bot and εm.top). The strains εs.top and εs.bot may exhibit compression (−ve) or tension (+ve) based on where the neutral axis is located. The neutral was located at a distance C from the top fiber using a computer spreadsheet and a trial-and-error technique. After locating the neutral axis, the ultimate moment (Mu) of a section can be found by obtaining the moment about the compressive force's application point in the manner described below

$$Mu = \Sigma Tri \times (di - \frac{C}{2}), \tag{19}$$

Equation (20), which depicts a simply supported beam subjected to a central concentrated load, can be used to calculate the ultimate load (Pu1)

$$Mu = \frac{Pu1}{4} \times Leffective, \tag{20}$$

where $L_{\text{effective}}$ = the effective span of the test specimen. Pu1 = the ultimate load for flexural failure.

Equation (21) was used to determine the ultimate shear strength, Qu, of the various designations, taking into account the specimen's shear failure

$$Qu = 0.24\sqrt{fcu} \times B \times d + Fym \times Ameshweb \times N \tag{21}$$

$$Pu2 = 2Qu, \tag{22}$$

where d = the effective depth of the beam.

A mesh web = the cross-sectional area of the web mesh reinforcement in the vertical direction within a length equal to (*d*).

N = number of webs.

Pu2 = the ultimate load for shear failure.

The smaller of Pu1 and Pu2 determines the failure mechanism and failure load of the beams. If Pu1 is the smaller of the two numbers, the failure mode is flexure; if not, the failure mode is shear. Based on the geometric and material parameters of each specimen, the

corresponding ultimate load was determined. The experimental-to-projected ratios for the ultimate loads of the beams under study are shown in Table 7. The table shows that for the majority of the examined beams, the theoretical ultimate loads and the experimental values coincide fairly well. The range of the ratio between the predicted and experimental ultimate loads was 0.93–1.07.

6 Finite-Element Modeling

The ABAQUS/CAE program was used to model and analyze each specimen (ABAQUS Documentation User's Guide, 2021). The validity of the created finite-element models was assessed using the experimental data.

6.1 Specimens Modeling

As depicted in Fig. 10a, nonlinear finite-element analysis (NLFEA) was used to estimate the behavior of composite beams made of ferrocement. The final capacity, deflection, and crack pattern of each specimen were among the behaviors that were discussed.

6.2 Elements' Description

6.2.1 Solid Element

Brick elements illustrated in Fig. 10b (C3D8R) were used to model concrete beams. There are three degrees of freedom in transition at each node of the element. This element was chosen, because it has the ability to specify both the contact faces required to apply loading as well as the bounds of the RC plate property. Furthermore, it accurately implements the constitutive law integration, is well suited for nonlinear static and dynamic analysis, and permits finite strain and rotation in large-displacement

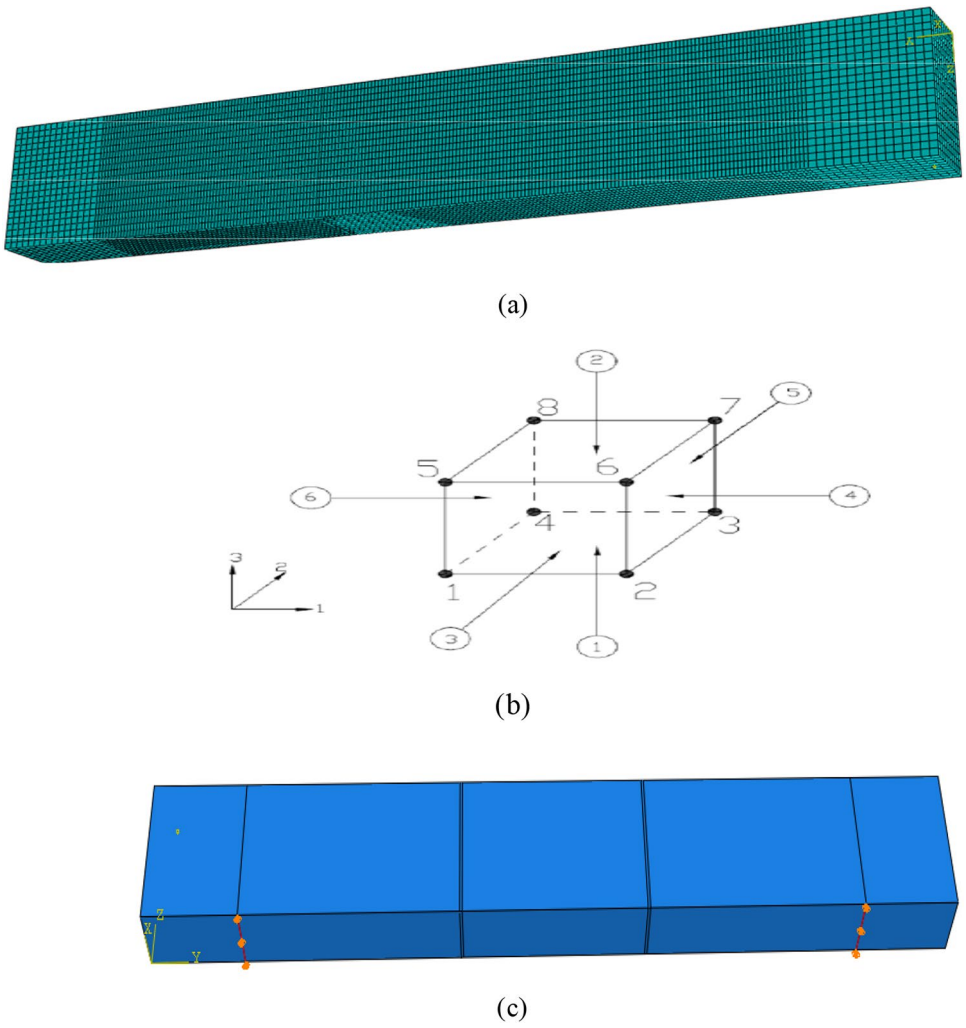

Fig. 10 Modeling of model parts

analysis. Impactor was also represented by a C3D8R element.

6.2.2 Truss Element

(T3D2) element was chosen in modeling reinforcement bars that were modeled as embedded elements in concrete block, because truss elements are rods that can only carry tensile or compressive forces and have no resistance to bending.

6.3 Material Properties

This section shows the material qualities for concrete, foam (EFC), reinforcing steel bars, and expanded and welded wire mesh.

The following inputs represent the material characteristics constants for concrete.

Poisson's ratio ($\mu = 0.3$) and the modulus of elasticity ($Ec = 4400\sqrt{fcu} = 24100\ N/mm^2$) (E.C.P., 2020).

Foam in Abaqus employs the following characteristics: Young modulus (E11, E22, E33), Poisson ratio (u12, u13, u23), shear modulus (G12, G13, G23), and stress limit (suboption-fail stress) in the individual axes and plains. Constants needed for defining the material were entered into the software according to the material definition. The foam properties are as follows:

Parameter	Value
1. Density, kg/m^3	36
2. Modulus of elasticity (E11), MPa	37.5
3. Modulus of elasticity (E22), MPa	23.5
4. Modulus of elasticity (E33), MPa	30.5
5. Poisson's ratio (υ12)	0.43
6. Poisson's ratio (υ13)	0.36
7. Poisson's ratio (υ23)	0.51
8. Shear modulus (G12), MPa	12.1
9. Shear modulus (G13), MPa	15.5
10. Shear modulus (G23), MPa	13.5
11. Compressive strength KPa	415

The following are the additional material qualities that are input for reinforcing steel:

1. Es = 200 k N/mm^2 is the elastic modulus of elasticity.
2. Yield stress (240 N/mm^2 and 360 N/mm^2 for fy and fyst).
3. The Poisson ratio, where $\mu = 0.2$.
4. A steel area of $2^{\phi}10$ (As = 157.07 mm^2).

The following inputs are used for the expanded wire mesh material properties:

1. Stress of yield (fy = 250 N/mm^2).
2. The diamond is 18 by 35 mm and has a 1.25 mm thickness.
3. One layer of increased mesh's volumetric ratio (V = 0.0093).
4. The extended mesh's two layers' volumetric ratio (V = 0.0186).

The following input represents the material parameters for welded wire mesh:

1. Stress of yield (fy = 400 N/mm^2).
2. The aperture measures 12.5 × 12.5 mm, and the wires have a 0.8 mm diameter.
3. Volumetric ratio (V = 0.0032) of an enlarged mesh layer.
4. Two-layer enlarged mesh volumetric ratio (V = 0.0064).

6.4 Finite-Element Results

Finite-element evaluations of the generated models examine beam failure strength, yielding of the reinforcing steel, and cracking. The nonlinear response is computed using the Newton–Raphson analysis approach. The loading was raised step-by-step until un-convergence, or failure. A summary of the finite-element analysis estimates, including the final loads and deflection, is shown in Table 6.

Table 6 Finite-element analysis results

Group	Specimens designation	F.C.L, KN	Ult. load, KN	Def. at first crack load, mm	Deflection at ult. load, mm	Ductility index
D	D1	14.63	48.78	1.30	12.54	9.64
	D2	14.83	51.38	1.18	13.75	11.65
E	E1-1E	12.8	46.53	1.02	9.74	9.55
	E2-2E	15.3	55.64	1.21	12.03	9.94
	E3-2W	14.4	52.33	1.25	11.33	9.06

The ultimate loads of each beam are displayed in Table 6. Control beams D1 and D2 have ultimate loads of 48.78 and 51.38 KN, respectively. The final loads on the beams E1, E2, and E3 were comparatively greater than the control.

Additionally, Table 6 displays the total beam deflection. The deflection for D1 and D2 in group D are 12.54 and 13.75 mm, respectively. In comparison to the control beams in group D, the deflection of the beams in group E reported lower values of deflection. Because specimen E2 had two layers of expanded wire mesh for reinforcement, it had a high deflection value of 12.03 mm at group E.

6.5 Cracking Patterns and Mode of Failure

Fig. 11 displays the cracking patterns and modes of failure for all specimen finite-element models. Flexural weakness caused the collapse of every specimen.

7 Comparison of the Outcomes of the NLFEA and the Experiments

The comparison of experimental and nonlinear finite-element data aims to confirm the suitability of NLFE models to represent the behavior and response of reinforced concrete beams.

In terms of ultimate deflection, ultimate load, and crack pattern, the results of the experiments and the five analytical models were compared.

7.1 Ultimate Load

Table 7 shows that the analytical ultimate load obtained from the NLFE program, and the experimental ultimate load coincide satisfactorily. The ratio between the experimental ultimate loads and the NLFE ultimate loads spans from 0.97 to 1.04, with an average ratio of 1.005. This confirms that the NLFE is capable of predicting the load-carrying capacity of ferrocement beams with light-weight core material.

7.2 Ultimate Deflection

Table 7 demonstrates that there is a satisfactory consensus between the experimental ultimate deflection and the analytical ultimate deflection produced from the NLFE program. With an average ratio of 0.96, the ratio between the NLFE ultimate deflections and the experimental ultimate deflections ranges from 0.94 to 0.98. This confirms that the NLFEA is capable of predicting the ultimate deflection of ferrocement beams with light-weight core material.

7.3 Comparison of Load–Deflection Curves

Fig. 12 shows the comparison between experimental and analytical load–deflection curves for all specimens.

7.4 Crack Patterns

By comparing the shape of the cracks in Fig. 8 to the shape of the cracks in Fig. 11 for the different samples, it can be noticed that there is a good match in the shape of the cracks, their direction, and their locations between the practical and the theoretical. This confirms that there is agreement between the practical program and the theoretical model. For example, Fig. 13 shows a comparison example where the cracking of NLFE was similar to the cracking pattern observed during experimental testing; these cracks started as micro-cracks in flexural and grew in length and width until failure as a flexural failure.

8 Conclusions

The following is a summary of the primary conclusions:

1. Especially, for buildings with intricate shapes and curves, welded and expanded wire meshes offer several advantages over steel reinforcement, including being lighter, easier to handle, easier to cut, and easier to bend.
2. The largest ultimate load and maximum deflection are found in ferrocement specimens with EFC core material and two layers of EMM reinforcement. These specimens outperform the conventionally reinforced concrete specimen (control specimen D1) by 11.38% and 2.92%, respectively.
3. In comparison to the control specimen, using expanded or welded wire mesh in place of steel stirrups shows a high ultimate load at a rate ranging from 6.78 to 11.38%.
4. Expanded wire mesh contributed to increased load-carrying capacity and deflection compared to welded wire mesh.
5. The ultimate load and load–deflection of ferrocement beams were enhanced by adding more layers of expanded and welded wire meshes.
6. When comparing beams reinforced with steel reinforcement to those strengthened with steel meshes, more and narrower cracks were seen.
7. The experimental and analytical results obtained for the ultimate failure load and deflection of ferrocement beams show a respectable agreement.
8. The limitation of the present work is that complete mortar coverage was given priority during construction, because incomplete mortar coverage might cause steel meshes to corrode.
9. It can be recommended to study the same parameter in the present work for long-term effects of the working load on the proposed beam system, such as creep and long-term deflection, and study the position of the different mesh of the net around the beam section.

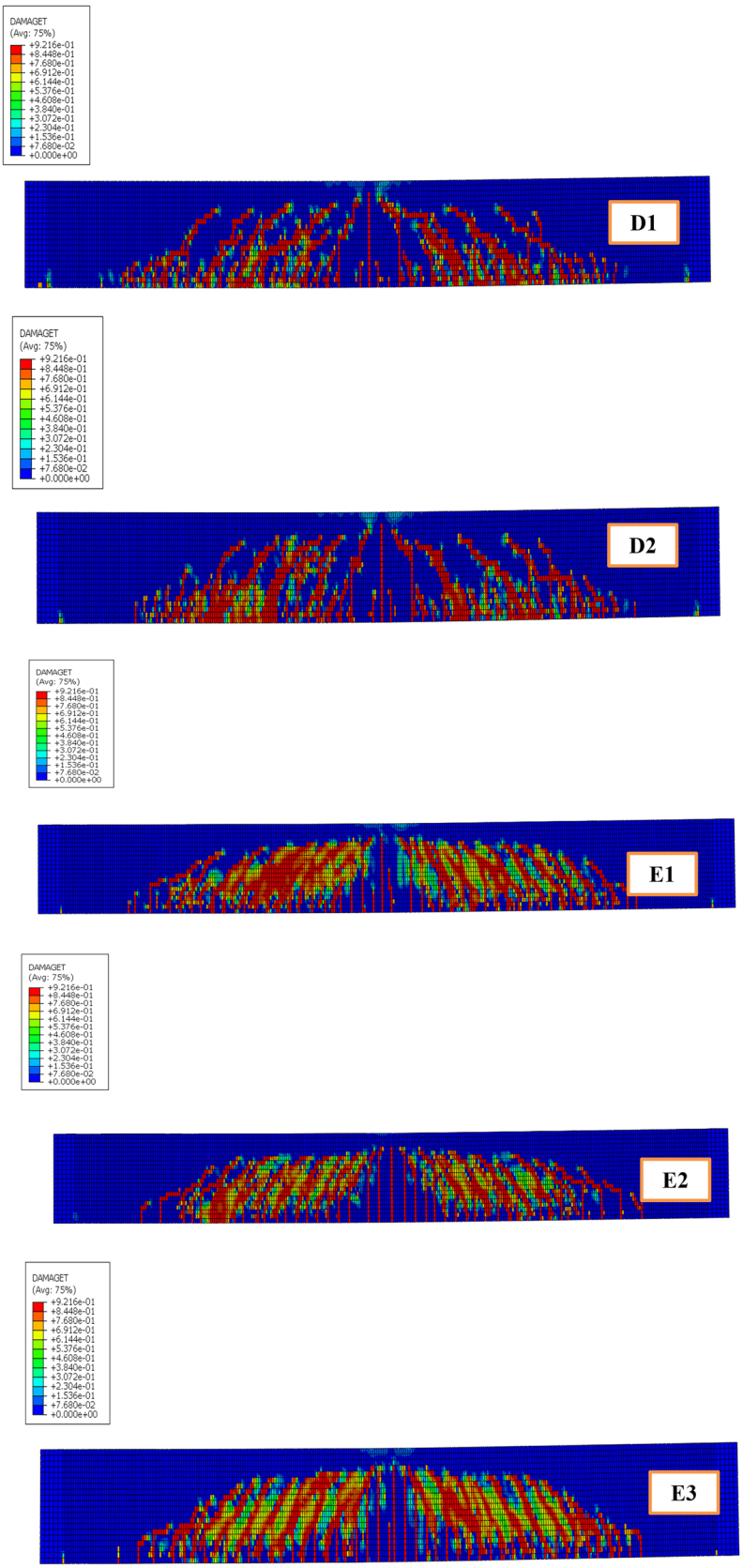

Fig. 11 Cracking patterns for finite-element models

Table 7 Comparison between experimental and NLFEM analysis

Sample ID	EXP						NLFEM				Pult,NLFEM /Pult,EXP
	1st Crack load, (KN)	Def.at 1st crack load, (mm)	Ultimate load, (KN)			Ult. def (mm)	1st Crack load, (KN)	Def.at 1st crack load, (mm)	Ultimate load, (KN)	Ultimate def (mm)	
			P exp	P prd	P exp./ P prd						
D1	14.87	1.49	47.25	44.15	1.07	12.96	14.63	1.30	48.78	12.54	1.03
D2	15.82	1.74	52.36	49.87	1.05	14.64	14.83	1.18	51.38	13.75	0.98
E1-1E	11.24	1.21	47.94	46.09	1.04	10.05	12.8	1.02	46.53	9.74	0.97
E2-2E	13.3	1.55	53.32	57.05	0.93	13.35	15.3	1.21	55.64	12.03	1.04
E3-2W	15.68	1.61	51.36	48.45	1.06	13.1	14.4	1.25	52.33	11.33	1.02

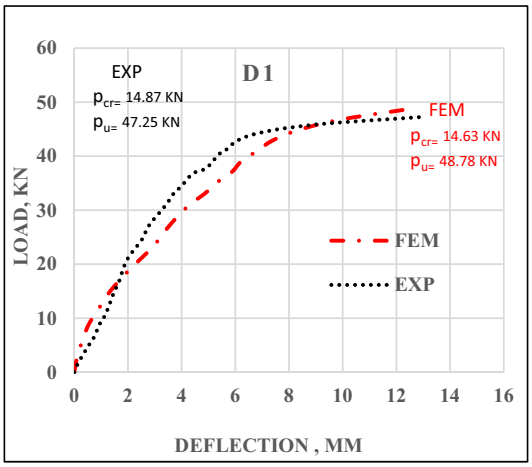

(a) Beam D1

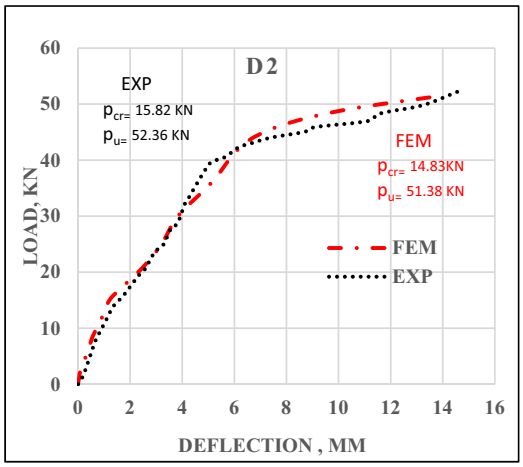

(b) Beam D2

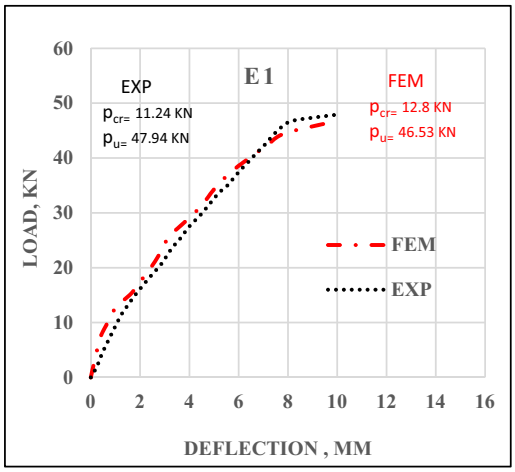

(c) Beam E1.

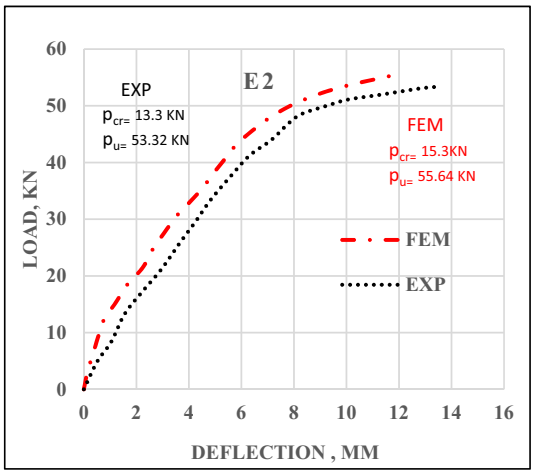

(d) Beam E2.

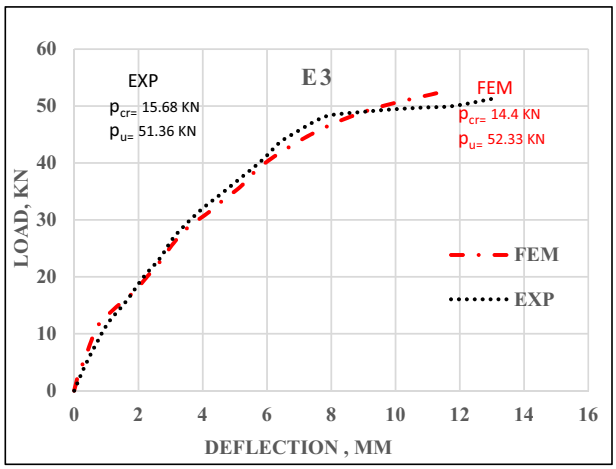

(e) Beam E3.

Fig. 12 Comparison between experimental and numerical load–deflection curves for all specimens

a) Experimental crack pattern

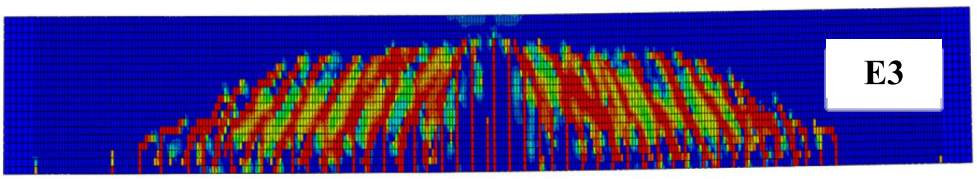

b) NLFEM crack pattern

Fig. 13 Sample of crack pattern for EXP& NLFEM

In the end, the failure load, deflection, and crack behavior are better affected by the ferrocement composite expanded or welded wire mesh used in the reinforcement of box sections as opposed to steel stirrups. Ferrocement is a versatile structural element that can be applied to a variety of strains. Hollow columns with horizontal stiffeners can be cast in ferrocement and used as a compression member. Ferrocement can be used to encapsulate walls or columns made of concrete, RCC, stone, or brickwork to strengthen them because of confinement. Membrane-stressed members, such as shells, domes, and pyramids, are easily cast in ferrocement, because the material is homogenous and the entire member is used to resist the membrane stresses.

Abbreviations

WWM	Welded wire mesh
EMM	Expanded metal mesh
EFC	Extruded foam core
NLFE	Nonlinear finite element
FEM	Finite-element model
F.C. L.	First crack load
E1-1E	Specimen E1 reinforced by one layer of expanded metal mesh
E2-2E	Specimen E2 reinforced by two layers of expanded metal mesh
E3-2W	Specimen E3 reinforced by two layers of welded wire mesh
R C	Reinforced concrete
ACI	American Concrete Institute
ASTM	American Society for Testing Materials
LVDT	Linear variable displacement transducer
Ast.bot.	Area of the steel bars at bottom of the beam
Ast.top	Area of the steel bars at top of the beams
Am.web	Area of the web steel mesh
Ac.m.bot.	Area of the steel mesh wrapping bottom of the core
Ac.m.top	Area of the steel mesh wrapping top of the core
Am.bot.	Area of the bottom steel mesh
Am.top	Area of the top steel mesh
Ari	Effective area of reinforcement either mesh or skeletal bars
$\eta_\circ$	Efficiency factor of reinforcement in the loading direction
AC	Cross-sectional area of ferrocement composite section
a	Depth of the compression block in the ferrocement matrix
B	Width of the specimen
C	Neutral axis depth from the top of the specimen
Es	Modulus of elasticity of the steel
Esth	Strain-hardening modulus of the steel
Fym	Yield stress of the steel mesh
Fu	Ultimate strength of the steel mesh
Fcu	Characteristic compressive strength of ferrocement mortar matrix
Cc	Internal forces in compression zone
Tr	Internal forces in tension zone

Acknowledgements
Not applicable.

Author contributions
M.A: performed the experimental program, numerical modeling, and original draft, M.H.M: designed the experimental program methodology, and performed the experimental program and final draft, M.H: numerical modeling, review, and editing. All authors read and approved the final manuscript, K. M. E: designed the experimental program methodology, performed the experimental program, and review and editing.

Funding
Open access funding provided by The Science, Technology & Innovation Funding Authority (STDF) in cooperation with The Egyptian Knowledge Bank (EKB).

Availability of data and materials
All data generated or analyzed during this study are included in this published article.

Declarations

Ethics approval and consent to participate
Not applicable.

Consent for publication
Not applicable.

Competing interests
There is no competing interest associated with the submission of this manuscript.

Received: 2 April 2024 Accepted: 3 February 2025
Published online: 12 May 2025

References

ABAQUS. (2021). Documentation User's Guide: ABAQUS User's Guide: Dassault Systems, Simulia Corp, Providence.

Abdullah, Q. N., & Abdulla, A. I. (2022). Flexural behavior of hollow self-compacted mortar ferrocement beam reinforced by GFRP bars. *Case Studies in Construction Materials, 17*, e01556. https://doi.org/10.1016/j.cscm.2022.e01556

Abdullah, Q. N., & Abdulla, A. I. (2023). Flexural behavior of a box ferrocement beams consisting of self-compacted mortar reinforced by fiber glass mesh and GFRP bars after exposure to high temperatures. *Journal of Building Engineering, 74*, 106917. https://doi.org/10.1016/j.jobe.2023.106917

ACI 549–1R-88. (2006). Guide for the design, construction, and repair of ferrocement. Manual of Concrete Practice, ACI Committee 549, Framington Hill: American Concrete Institute, 30.

ACI 549.1R-93 & ACI 549-1R-88, A. C. I. guide for the design construction, and repair of ferrocement, ACI Committee 549.1R-93; ACI 549-1R-88 and 1R-93.

Al-Shathr, B. S., Abdulhameed, H. A., & Mahdi, M. M. (2022). Effect of wire-mesh type on strengthening reinforced concrete beams. *Engineering and Technology Journal, 40*(05), 759–768. https://doi.org/10.30684/etj.2021.131159.1009

ASTM C 494/C494M. (2005). Standard Specification for Chemical Admixtures for Concrete.

ASTM C/150–07. (2007). Standard Specification for Portland Cement.

ASTM C778. Graded Sand ASTM 'Cement testing standard specifications for standard sand'.

ChandraSekharRao, T., GunneswaraRao, T., RamanaRao, V., & Rambabu, C. (2012). An experimental study on ferrocement flexural loading. *International Journal of Emerging Technology and Advanced Engineering, 2*(9), 138–144.

E.C.P. 203. (2020). Egyptian Code of Practice: Design and Construction for Reinforced Concrete Structures, Egypt Cairo.

Egyptian Standards Specification, E.S.S, 4756–11. (2012). Physical and mechanical properties examination of cement, part 1, Cairo.

Elkassas, E., Morsy, A. M., & Marzouck, M. (2022). Flexure behavior of hollow steel beams strengthening with ferrocement. *Journal of Engineering and Applied Science*. https://doi.org/10.1186/s44147-022-00123-2

El-Sayed, T. A., & Algash, Y. A. (2021). Flexural behavior of ultra-high performance geopolymer RC beams reinforced with GFRP bars. *Case Studies in Construction Materials, 15*, e00604. https://doi.org/10.1016/j.cscm.2022.e01054

El-Sayed, T. A., Deifalla, A. F., Shaheen, Y. B., Ahmed, H. H., & Youssef, A. K. (2023b). Experimental and numerical studies on flexural behavior of GGBS-based geopolymer ferrocement beams. *Civil Engineering Journal, 9*(3), 629–653. https://doi.org/10.28991/CEJ-2023-09-03-010

El-Sayed, T. A., Erfan, A. M., Abdelnaby, R. M., & Soliman, M. K. (2022). Flexural behavior of HSC beams reinforced by hybrid-GFRP bars with steel wires. *Case Studies in Construction Materials, 16*, e01054. https://doi.org/10.1016/j.cscm.2022.e01054

El-Sayed, T. A., Shaheen, Y. B., AbouBakr, M. M., & Abdelnaby, R. M. (2023c). Behavior of ferrocement water pipes as an alternative solution for steel water pipes. *Case Studies in Construction Materials, 18*, e01806. https://doi.org/10.1016/j.cscm.2022.e01806

El-Sayed, T. A., Shaheen, Y. B., Mohamed, F. H., & Abdelnaby, R. M. (2023a). Performance of ferrocement composites circular tanks as a new approach for RC tanks. *Case Studies in Construction Materials*. https://doi.org/10.1016/j.cscm.2023.e02228

El-Wafa, M. A., & Fukuzawa, K. (2010). Characteristics of ferrocement thin composite elements using various reinforcement meshes in flexure. *Journal of Reinforced Plastics and Composites*. https://doi.org/10.1177/0731684410377814

Eskandari, H., & Madadi, A. (2015). Investigation of ferrocement channels using experimental and finite element analysis. *Engineering Science and Technology, an International Journal, 18*, 769–775.

Fahmy, E. H., Shaheen, Y. B. I., Abdelnaby, A. M., & Zeid, M. N. A. (2014a). Applying the ferrocement concept in construction of concrete beams incorporating reinforced mortar permanent forms. *International Journal of Concrete Structures and Materials, 8*(1), 83–97. https://doi.org/10.1007/s40069-013-0062-z

Fahmy, E. H., Shaheen, Y. B. I., Abdelnaby, A. M., & Zeid, M. N. A. (2014b). Applying the ferrocement concept in construction of concrete beams incorporating reinforced mortar permanent forms. *International Journal of Concrete Structures and Materials*. https://doi.org/10.1007/s40069-013-0062-z

Gaidhankar, D. G., Kulkarni, M. S., & Jaiswal, A. R. (2017a). Ferrocement composite beams under flexure. *Int Res J Eng Technol, 04*(10), 117–124.

Gaidhankar, D., Kulkarni, M., & Jaiswal, A. (2017b). Ferrocement composite beams under flexure. *International Research Journal of Engineering and Technology, 4*(10), 117–124.

Gandomi, A. H., Roke, D. A., & Sett, K. (2013). Genetic programming for moment capacity modeling of ferrocement members. *Engineering Structures, 57*, 169–176. https://doi.org/10.1016/j.engstruct.2013.09.022

Kaish, A. B. M. A., Jamil, M., Raman, S. N., Zain, M. F. M., & Nahar, L. (2018). Ferrocement composites for strengthening of concrete columns: a review. *Journal of Construction and Building Materials, 160*, 326–340. https://doi.org/10.1016/j.conbuildmat.2017.11.054

Makhlouf, M. H., Alaa, M., Khaleel, G. I., Elsayed, K. M., & Mansour, M. H. (2024). Shear behavior of reactive powder concrete ferrocement beams with light weight core material. *International Journal of Concrete Structures and Materials, 18*, 46. https://doi.org/10.1186/s40069-024-00684-x

Mhadeshwar, S.N., & Naik, A. M. (2017). Experimental performance, mathematical modelling and development of stress block parameter of ferrocement beams with rectangular trough shaped skeletal steel. *International Research Journal of Engineering and Technology* 1387–1393 e-ISSN: 2395–0056.

Shaaban, I. G. (2002). Expanded wire fabric permanent formwork for improving flexural behaviour of reinforced concrete beams. Composite Materials in Concrete Construction: Proceedings of the International Seminar held at the University of Dundee, 59–70. https://doi.org/10.1680/cmicc.31746.0006

Shaaban, I. G., Shaheen, Y. B., Elsayed, E. L., Kamal, O. A., & Adesina, P. A. (2018a). Flexural characteristics of lightweight ferrocement beams with various types of core materials and mesh reinforcement. *Construction Building Materials, 171*, 802–816. https://doi.org/10.1016/j.conbuildmat.2018.03.167

Shaaban, I. G., Shaheen, Y. B., Elsayed, E. L., Kamal, O. A., & Adesina, P. A. (2018b). Flexural behaviour and theoretical prediction of lightweight ferrocement composite beams. *Case Studies in Construction Materials*. https://doi.org/10.1016/j.cscm.2018.e00204

Shaheen, Y. B. I., El-Sabbwy, M., & El-Bordeny, D. A. H. (2022). Structural characteristics of lightweight ferrocement beams with different core material. *Journal of Engineering Research and Reports, 23*(6), 30–52. https://doi.org/10.9734/jerr/2022/v23i617616

Shaheen, Y. B., Hekal, G. M., & Elshaboury, A. M. (2022). Structural behavior of ferrocement i-beams with web openings: experimental study. *Engineering Research Journal, 45*(4), 581–589. https://doi.org/10.21608/erjm.2022.146160.1188

Usman, F., & Shaharudin, M. S. (2018). Effect of polypropylene fibres on torsional strength of ferrocement. *Indian Journal of Science and Technology*. https://doi.org/10.17485/ijst/2018/v11i8/114093

Yardim, Y. (2019). Review of research on the application of ferrocement in composite precast slabs. *Periodica Polytechnica Civil Engineering, 62*(4), 1030–1038. https://doi.org/10.3311/PPci.11737

M. Alaa is a Ph.D. Student, Civil Engineering Department, Benha Faculty of Engineering, Benha University, Egypt.

Mohamed H. Makhlouf is a Professor, Civil Engineering Department, Benha Faculty of Engineering, Benha University, Egypt.

M. H. Mansour is an Associate Professor, Civil Engineering Department, Benha Faculty of Engineering, Benha University, Egypt.

K. M. Elsayed is a Professor, Civil Engineering Department, Benha Faculty of Engineering, Benha University, Egypt.